

# Feature Extraction in Laser Welding Processes

Marc Geese\*, Ronald Tetzlaff<sup>§</sup>, Daniel Carl<sup>†</sup>, Andreas Blug<sup>†</sup>, Heinrich Höfler<sup>†</sup> and Felix Abt<sup>‡</sup>

\*Johann Wolfgang von Goethe University  
Frankfurt am Main, Germany  
Email: marc@geese-online.de

<sup>†</sup> Fraunhofer Institute for Physical Measurement Techniques IPM  
Freiburg, Germany

<sup>‡</sup> Forschungsgesellschaft für Strahlwerkzeuge mbH (FGSW)  
Stuttgart, Germany

<sup>§</sup> Technische Universität Dresden  
Dresden, Germany

**Abstract**— There is a rapidly growing demand for laser welding in a wide variety of manufacturing processes ranging from automobile production to precision mechanics. Up to now, the high dynamics of the process has made it impossible to construct a camera based real time quality and process control. Since new pixel parallel architectures are existing, which are now available in systems such as the ACE16k [1], Q-Eye [1], and SCAMP-3 [2], one has become able to implement a real time laser welding processing.

In this paper we will propose a feature extraction algorithm, running at a frame rate of 10 kHz, for a laser welding process. The performance of the algorithm has been studied in detail.

In particular, it has been implemented on an Eye-RIS v.1.1 system and has been applied to laser welding processes.

## I. INTRODUCTION

### A. About the project

Many industries are using laser welding processes in their manufacturing lines [3]. Because no camera based fast process control exists, there is no adequate possibility of correcting a process after it has been started. The number of defective goods can be reduced by means of a real time visual process control. Especially a detection of errors in the welding process would be worth the effort, because an additional quality control unit would not be required and one could purchase the result immediately once the process is completed.

### B. Laser welding processes

In laser welding processes the beam power of a laser is employed to melt the material. In our investigation, we have taken two plates of iron in a lap joint. The plates are 0.7 mm thick, with a gap of 0.1 mm. The laser is a Yb:YAG thin disk laser which has an optical output power of 6000 W at a wavelength of 1030 nm.

1) *Theoretical concept of the process:* In Fig. 1 is sketched a cross section of the laser welding process and the resulting image of the melt. The image is obtained using telescope optics incorporated in the confocal optics of the laser welding head. It shows the thermal radiation of the melt in the spectral range of 820 nm to 980 nm.

At the moment when the beam interacts with the material, it vaporizes instantly, generating metal vapor. Underneath the

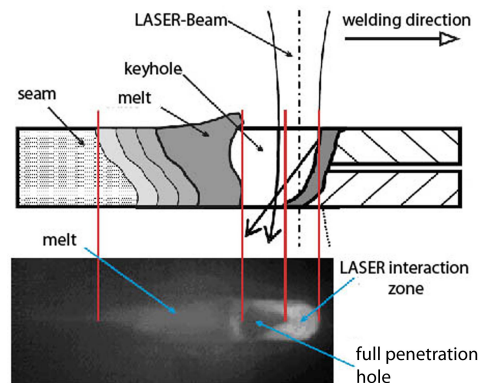


Fig. 1. Schematics of a welding process with lap joint

metal vapor, the beam starts to melt the solid material. The metal vapor creates hydrostatic pressure and starts to penetrate the molten material underneath. Due to the pressure of the metal vapor and the motion of the interaction zone of the beam, the melt is forced generally to move in the opposite direction to the welding direction.

The zone of metal vapor subsequently expands deeply inside the material, resulting in molten material in all plates of the welding setup. Consequently, a hole in the material is created and remains open and stable due to the hydrostatic pressure of the metal vapor. The zone of metal vapor is called the *keyhole*.

As can be seen in Fig. 1, the keyhole is inclined towards the welding direction. This occurs because the melting takes some time and the beam is moving fast. Deeper areas are therefore vaporized later, leading to the inclination of the keyhole. If the beam power is strong enough and the welding speed is slow enough, the keyhole may penetrate until it crosses the last plate. Then the process is said to have full penetration. A fully penetrated process ensures that the two materials are connected properly after resolidification and thus it is an important quality feature.

2) *Image acquisition:* Image acquisition of the process is realized by a beam splitting cube coupling coaxially in the optic path of the welding laser. A telescope optic is used in

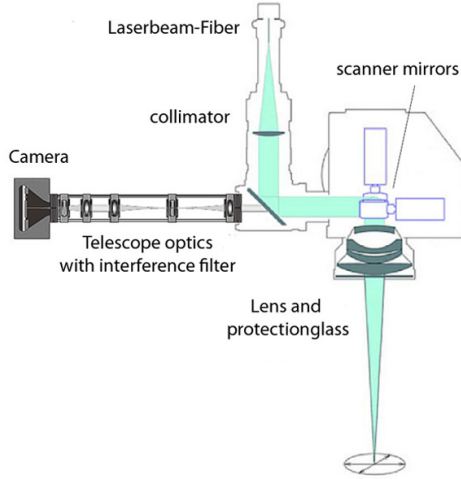
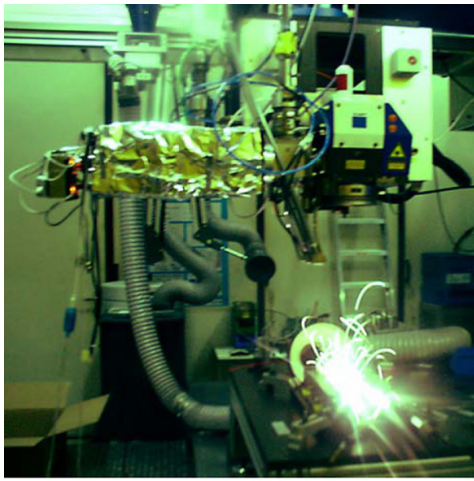


Fig. 2. Experimental setup to watch the welding process

order to adapt the optical magnification to the size and pixel pitch of the respective sensor array. In addition, an interference filter cuts out the spectral range from  $820\text{ nm}$  to  $980\text{ nm}$ . As a result, mainly the heat radiation of the process will be observed by the sensor. Sample images of the laser welding process received with two different camera systems are depicted in Fig. 3 and Fig. 4.

3) *Process related features of the acquired images:* The next step is to find out which quality features can be found in the images that have been acquired by the experimental setup shown in Fig. 2.

Many pictures of different welding processes have been recorded using the experimental setup. As a result it is possible to match the recorded images to the theoretical concept of the welding process described above (I-B.1).

A large number of quality features were observed in the images. The most important quality feature is full penetration. A visual illustration can be seen in Fig. 5.

A very intense circular area can be seen, which involves the interaction zone between the metal and the beam. Directly behind the interaction zone, a dark triangular shaped area is observed. This area is the projection of the zone where the

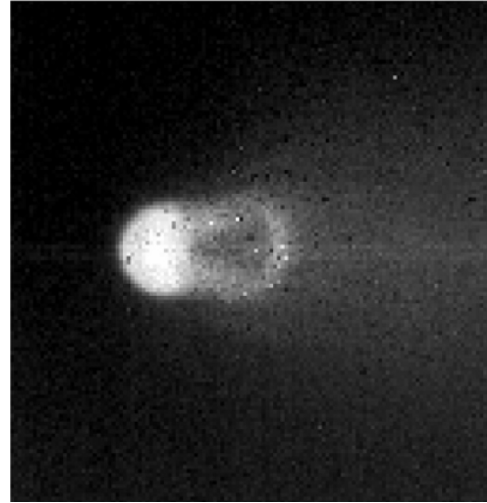


Fig. 3. An image acquired by the ACE16k focal plane processor and an exposure time of  $t_{exp} = 580\ \mu s$

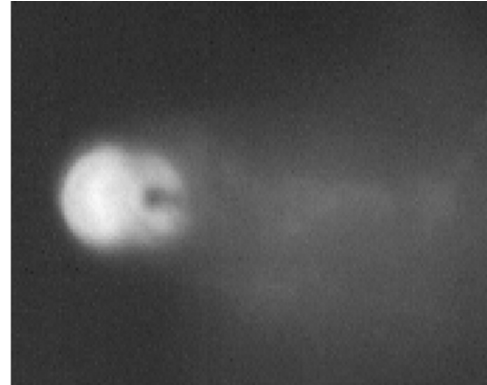


Fig. 4. An image acquired by the Q-Eye focal plane processor and an exposure time of  $t_{exp} \approx 50\ \mu s$

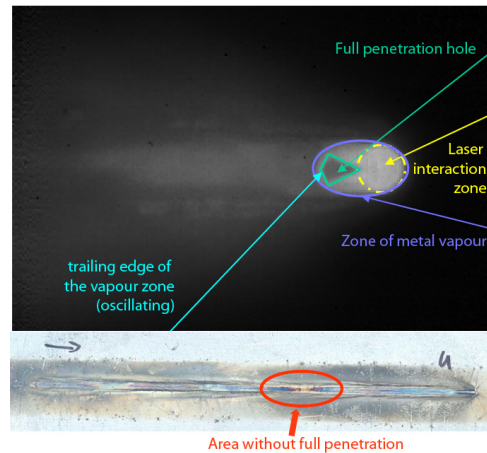


Fig. 5. The full penetration hole and a typical welding seam. In the marked area the process had no full penetration hole

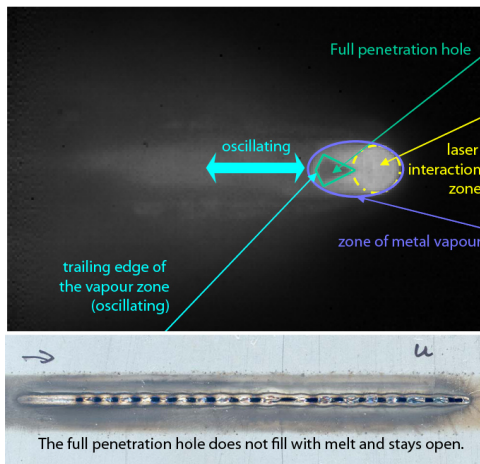


Fig. 6. The oscillating edge of the keyhole causes holes in the welding seam

keyhole totally penetrates the metal plates. Owing to the fact that the metal vapor does not radiate within the  $820\text{ nm}$  to  $980\text{ nm}$  wavelength area, dark areas are observed. At the upper and lower borders of the triangle, some intense areas can be seen which fade out with their distance from the interaction zone. These areas contain melt and possibly some metal vapor above it. The cooler the melt the darker its image becomes.

The dark triangle is called the full penetration hole. If the full penetration hole becomes visible, one can be sure that the process works in such a way that both pieces will have a good connection after resolidification. This is evident from the welding seam below the image in Fig. 5. A part where full penetration did not occur has been marked and it can be seen that the welding seam looks differently.

Fig. 6 shows a quality feature that is related to process dynamics. The rear edge of the full penetration hole may fall backwards or may begin to oscillate if the welding speed is faster than the ability of the melt to fill the keyhole or if the gap between the two plates of iron is too wide. As a result, the melt fills that gap between the plates and no material is left to fill the keyhole.

Then the keyhole elongates and the longer the keyhole becomes the instability increases. This results from the ability of the metal vapor to leave the keyhole over a wide area. If the keyhole becomes too unstable, it collapses and leaves a hole in the workpiece.

Other quality features tweaked in this paper are spatters. In Fig. 7 spatters are marked that fly away from the process. Note the change in zoom for this image. Spatters occur for many reasons. The main reason in lap joint weldings with zinc coated plates is a small gap according to the thickness of the plates. The process contains a large quantity of melt in this case which leads to a very short keyhole. The zinc vapor cannot leave through the gap and escapes through the small keyhole. Since in this case the vapor streams out rapidly, it carries the melt away. Then two main problems arrive. The first concerns the missing metal that has been expelled. If a large number of spatters are detected, holes in the welding

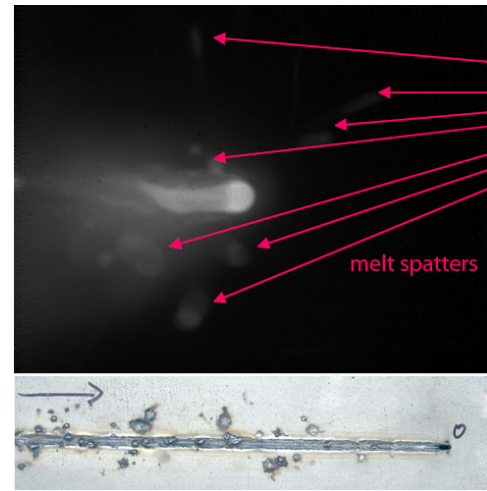


Fig. 7. Spatters in the process and as a result a contaminated workpiece

seam may occur because insufficient melt remains to fill the keyhole.

The second problem arrives in the wide field of precision mechanics, where the workpiece needs to be kept clean. Spatters can land on the workpiece next to the welding seam, as shown in Fig. 7. Contamination of the workpiece can make it useless for further manufacturing.

Each feature can be influenced by a certain set of parameters. For example, the full penetration hole can be influenced by the beam power, while the oscillating edge is dependent on the welding speed. The appearance of spatters is still under investigation, but however there seems to be a correlation between the welding speed and the amount of spatters.

### C. Requirements for a real time control system

As mentioned before, we wish to develop a real time control system in order to prevent errors in a welding process. Various different quality features can be used to obtain a clearer image of the process details. With a fast process control errors can be corrected during resolidification. However, we need to react within extremely short time. Consequently very high frame rates and short processing times are needed.

Many of the hardware applications of Cellular Neural Networks (CNN) are implemented as Focal Plane Processors (FPPs). These realizations contain a small computing device for each pixel, which allow data processing massively in parallel. This high performance makes it possible to achieve image processing within a required time of  $100\ \mu\text{s}$ .

Furthermore, the structure of the FPPs is similar to the structure of CNNs because individual cells are interconnected. Consequently CNN model-based algorithms can be transferred easily to FPP processors. In order to achieve a high frame rate, image sensors are required with high sensitivity in the wavelength area of  $820\text{ nm}$  to  $980\text{ nm}$ .

In order to observe the full dynamics of the process, high frame rates of  $10\text{ kHz}$  ( $100\ \mu\text{s}$  processing time) have to be performed. Lower frame rates lead to missing data in between

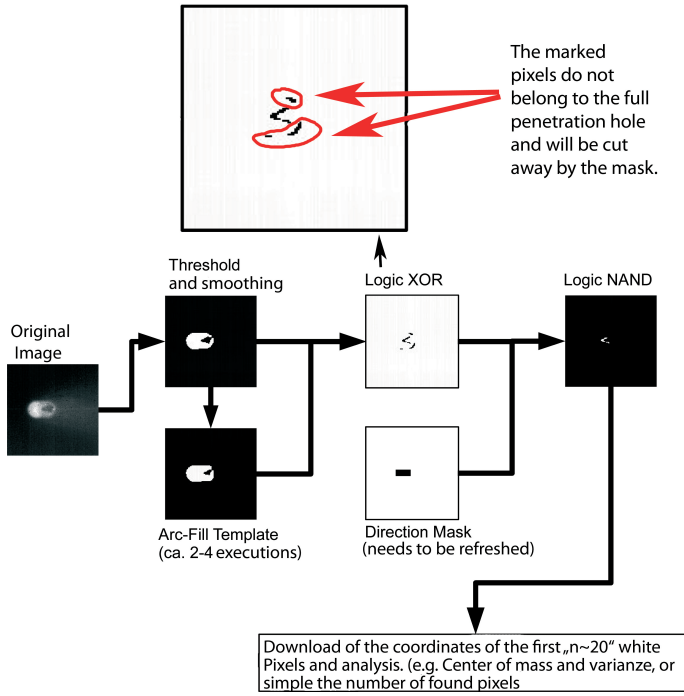


Fig. 8. The ArcFill algorithm for the ACE16k

images, thus resulting in the impossibility to discover effects occurring between two images.

## II. HARDWARE AND ALGORITHMS

This paper we will be focused on the full penetration hole together with experimental results of the detection of the full penetration hole.

### A. Algorithms for feature extraction

1) *The ArcFill-algorithm:* The first step was to devise algorithms that could detect the full penetration hole. Owing to the real time conditions an algorithm had to extract the full penetration hole within  $100 \mu s$ . It can readily be seen that those algorithms must be adapted to the hardware used in order to achieve maximum performance. We applied an ACE16k v.2 in our tests. This chip is available in the Eye-RIS v.1.1 system. Fig. 3 shows an image taken using the ACE16k. It can be seen that the image contains a large number of noise pixels which should be considered in the algorithms. We developed algorithms inspired by CNNs and attempted to use only a very small number of CNN templates. A flow chart of the fastest algorithm that has been found for the ACE16k is shown in Fig. 8.

The first step of this algorithm transfers the image into a binary image with a constant threshold. By extensive statistical analysis it could be verified that it is possible to use a constant threshold value for each experimental setup. After thresholding the full penetration hole becomes visible in the binary image. The next stage was to fill the full penetration

hole with a special "ArcFill"-template. The ArcFill-template is a propagating template.

These templates are quite slow on the ACE16k. Therefore it was applied for no more than 4 time steps. Subsequently a logical XOR operation is used with the thresholded image and the filled image. This procedure leads to an image that contains the hole. Unfortunately, the ArcFill-template fills the diagonal edges as well, as can be seen in Fig. 8.

We are aware that the full penetration has to be beyond the beams interaction zone, which has a fixed position in each setup. Additionally the full penetration hole cannot be wider than the interaction zone. Therefore we can use a mask to cut away most of the wrong pixels originating from the diagonal edges. After this step the coordinates of the first 20 white pixels from the image are downloaded.

Using this information a control signal for the welding machine can be calculated.

2) *Reliability of the algorithm:* This algorithm has been tested for its correct classification rate. Special software has been programmed, which compares the result of a human specialist with the result of the algorithm. A random sample of over 1000 images covering all threshold values and images of every welding setup has been evaluated. Consequently we can say that we achieve a correct classification rate of  $\geq 90\%$ . The  $\alpha$ -error of our test was  $\leq 0.5\%$ . Our test had a statistical power of  $\beta \geq 95\%$ . More than 50% of the test images will very unlikely appear in an actual application. Therefore, further research should result in a number larger than 90% for the lower border.

### B. Available Hardware

As already mentioned, the algorithm has been implemented on Eye-RIS v.1.1 hardware. The processing time for an acquired image is  $97.2 \mu s$ . Owing to the ACE16ks image sensors (see Fig. 3), it has been necessary to modify the algorithm. Initially we used a special threshold-operation with the average value of a  $3 \times 3$ -neighborhood for thresholding. This operation takes as long as the usual threshold and has the advantage of a smoothing effect. Additionally, it was necessary to implement an "opening" operation, that slows the algorithm down to  $5 kHz$  or  $6 kHz$ , depending on how often it is applied. This is necessary in order to smooth the edges of the thresholded image. The Arc-Fill-Template will work more reliable with smoothed edges. The next image is acquired alongside processing. In order to obtain an image, the sensors must be exposed for  $580 \mu s$ . Hence one must wait for the difference of exposure time and processing time before one can start the processing. This leads to an output frame rate of  $1.6 kHz$  instead of  $10 kHz$ .

This slowdown only depends on the sensitivity of the optical sensors and the resulting image quality of the Eye-RIS v.1.1 System. The system would be able to work with the demanded  $10 kHz$  if better sensors were available. A considerable improvement in performance is expected by use of the new Q-Eye processor. As an initial result Fig. 4 shows an image obtained by the Q-Eye with an exposure time of only

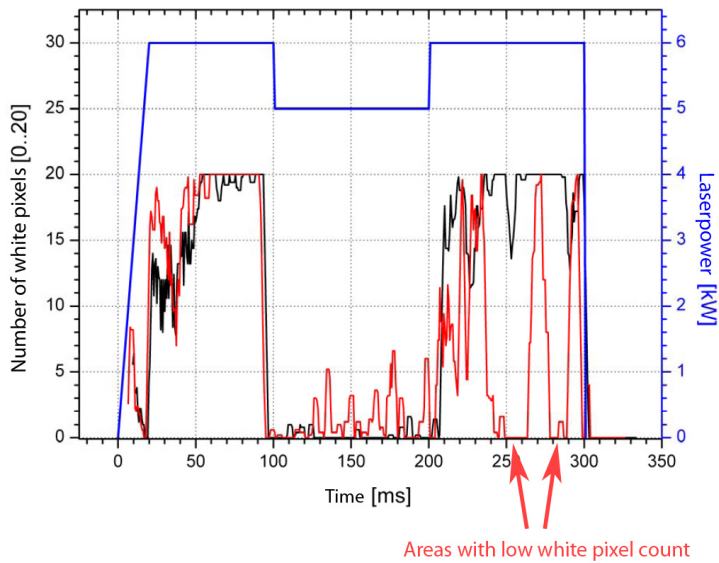


Fig. 9. Results of the ArcFill-algorithm of two test weldings. The welding seams can be seen in Fig. 10

$t_{exp} \approx 50 \mu s$ . This short exposure fully cancels the necessary slowdown of the Eye-RIS v.1.1 System and frame rates of  $10 kHz$  become realizable. Future research will be performed with the Q-Eye processor.

### III. TESTING IN A REAL WELDING PROCESS

In the test on the welding machine, the implemented algorithm had to be slowed from  $10 kHz$  to  $1.6 kHz$  due to the exposure times and the modifications mentioned above. The result of the algorithm is a stream of the number of white pixels in the final images. Fig. 9 shows the result of two test weldings.

In both welding tests, the beam power has been modified during the process as indicated by the blue line. The red and black lines show the number of white pixels transferred by the algorithm. In both weldings it can be seen that the algorithm indicated that no full penetration welding has been achieved if the beam power had been reduced. You can see the welding seams of both tests in Fig. 10. Both welding seams show a difference when the beam power is reduced. In the case of the seam corresponding to the red line, the zone of no full penetration can be readily seen in the photograph. In the case of the seam originating from the black line, one must focus to the width of the welding seam and the different color in the middle in order to see the part without full penetration. Looking more closely at the red line it will be seen that the number of white pixels has two additional areas of low counts when the beam power already has returned to  $6 kW$ . Comparing this with the welding seam in Fig. 10(a), it will be seen that the welding seam has noticeable marks corresponding to the areas of low white-pixel count. These areas are similar to those in Fig. 5. In case of the red test welding, we were able to detect a process error that occurred even though all the parameters were correct. As mentioned

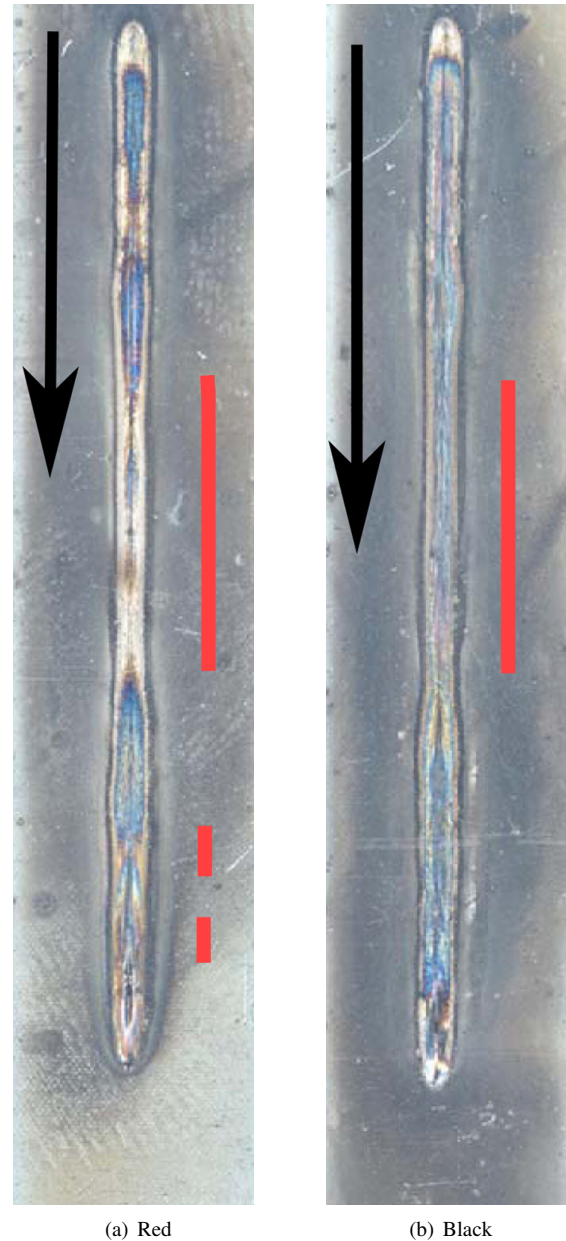


Fig. 10. The welding seams for the test welding shown in Fig. 9. Areas of lack of full penetration have been marked.

in the introduction these errors occur quite frequently. Main reasons are unevenness and soiling of the material - in addition to major fluctuations in the keyhole. Furthermore, the welding fumes have to be correctly dissipated, otherwise absorption and diffusion of the laser beam may inhibit full penetration.

### IV. CONCLUSION

CNN-based algorithms implemented on Focal Plane Processor architectures are capable to enhance industrial process controls. Satisfying results are available for detection of full penetration welding in laser welding processes. Currently algorithms that will detect some of the other quality features are under development. The new Q-Eye processor will be used

for further research, since it has sensors which need only  $\frac{1}{10}$ th of the exposure time of the ACE16ks sensors.

#### ACKNOWLEDGMENT

The authors would like to thank Claudia Baulig for her help in constructing the optics of the experimental setup and Anafocus the support with Eye-RIS systems and for useful advices.

All the results were obtained in the project "Analoge Bildverarbeitung mit zellularen neuronalen Netzen (CNN) zur Regelung laserbasierter Schweißprozesse (ACES)". This project is sponsored by the "Landesstiftung Baden-Württemberg" in the field "Forschung Optische Technologien 2005/20061"

#### REFERENCES

- [1] Company Anafocus, *Av. Isaac Newton s/n, Pabelln de Italia, Parque Tecnolgico Isla de la Cartuja*, 41092 Seville, Spain. [www.anafocus.com](http://www.anafocus.com).
- [2] P.Dudek, D.R.W.Barr, A.Lopich and S.J. Carey, *Demonstration of real-time image processing on the SCAMP-3 vision system*, IEEE International Workshop on Cellular Neural Networks and their Applications, CNNA 2006, pp.13-13, Istanbul, August 2006
- [3] Kogel-Hollacher, M. et al.: Camera based Process Monitoring of the CO<sub>2</sub> and ND:YAG Laser Welding Process: Experiences from Applications in the Automotive Industry. In: Proc. of the Lasers Materials Processing Symposium ICALEO2004, Orlando, Florida (LIA), 2004.
- [4] Cellular neural networks and visual computing, Foundations and applications, Leon O. Chua and Tams Roska
- [5] Mller-Borhanian, J. (Hrsg.): Integration optischer Messmethoden zur Prozesskontrolle beim Laserstrahlschweien (INESS); Abschlussbericht zum Verbundprojekt. Herbert Utz Verlag, Mnchen, 2005. ISBN 3-8316-0531-9